Cosmic-ray composition around 10^{18} eV

T. K. Gaisser, Todor Stanev, and Serap Tilav*

Bartol Research Institute, University of Delaware, Newark, Delaware 19716

S. C. Corbato, H. Y. Dai, B. R. Dawson,[†] J. W. Elbert, B. Emerson,
D. B. Kieda, M. Luo, S. Ko, C. Larsen, E. C. Loh, M. H. Salamon, J. D. Smith,
P. Sokolsky, P. Sommers, J. Tang, and S. B. Thomas

Department of Physics, University of Utah, Salt Lake City, Utah 84112

D.J. Bird

Physics Department, University of Illinois, Urbana, Illinois 61801

(Received 9 October 1992)

We use the depth of maximum distribution as measured by the stereo Fly's Eye detector to study the chemical composition of the primary cosmic radiation between 3×10^{17} eV and 10^{19} eV. The analysis depends on the use of simulations to study the response of the detector as well as sensitivity to assumptions about the properties of hadronic interactions that determine cascade development. We find that the incident particles include both heavy nuclei and protons in comparable amounts. The fraction of protons appears to increase at the highest energy explored.

PACS number(s): 96.40.De, 13.85.Tp, 95.85.Ry

I. INTRODUCTION

The chemical composition of the primary cosmic-ray nuclei puts an important constraint on models of cosmic-ray production and propagation. Recent results of the JACEE Collaboration [1] allow the composition to be summarized near 4×10^{14} eV total energy per particle. The value of $\langle \ln(A) \rangle$ is 2.33±0.27. The percentages of p, He, C-O, Ne-S, and $Z > 17$ were found to be 12±9, 25±14, 26±12, 15±8, and 21±10, respectively. In the energy region above 10^{15} eV, measurements of the composition are indirect and difficult and many models are possible. At about 3×10^{15} eV (the "knee" of the spectrum) the cosmic-ray spectrum steepens, with a power-law exponent changing from about -2.7 to -3.1. This may occur because an acceleration or confinement mechanism which depends on magnetic rigidity is less effective above an energy per particle which is proportional to the Z value of the accelerated nucleus. The spectrum would then be steeper for protons than for heavy nuclei, resulting in a mixed composition with a higher fraction of heavy nuclei than at energies below the knee.

At present, a commonly accepted model of particle acceleration below 10^{14} eV involves diffusive shock acceleration by supernovas [2-5]. Because the spectrum is continuous at the knee, it can be argued [6,7] that the spectrum beyond the knee results from the reacceleration of galactic cosmic rays previously accelerated by supernova shocks. In the model of Jokipii and Morfill [6] the reacceleration occurs at the galactic wind termination shock. Ip and Axford [9] attempt to reaccelerate cosmic rays at merging supernova remnants. In general, it is plausible that the composition from reacceleration processes would be roughly similar to the composition observed below the knee.

Völk and Biermann [10] point out that for shocks developing in high magnetic fields, e.g., in the presupernova stellar winds, the maximum energy at acceleration can exceed the energy of the knee for heavy high-Z nuclei. An application to specific presupernova stars [11] shows cosmic-ray composition enriched in certain elements with charge $Z > 1$. Another view, advocated by Jokipii [8], is that accounting for the geometry of the magnetic field relative to the supernova remnant can lead to higher estimates of the energy achievable when a supernova expands into the interstellar medium.

A very different result for the composition beyond the knee could result from a model proposed by Hillas [12]. Hillas pointed out the difficulty of matching the sharpness of the spectral break at the knee to models in which the knee is due to increased losses of particles with rigidities (pc/Ze) above a critical value. He suggested that if the acceleration occurred in an environment with high fluxes of photons the onset of photopion production energy losses (for protons) and photodisintegration (for Fe nuclei) would occur at similar values of energy per particle, and a relatively sharp spectral break could be produced at the knee. Because of the destruction of nuclei by photodisintegration, an enhanced fraction of protons could be present beyond the knee. A qualitatively simi-

*Present address: Department of Physics, University of Wisconsin, Madison, WI 53706.

†Present address: Department of Physics and Mathematical Physics, University of Adelaide, Adelaide, South Australia 5001.

lar picture follows from the suggestion [13] that a large fraction of the cosmic rays at and above the knee comes from the decay of neutrons that escape from active galactic nuclei (AGN's) after their parent protons (or heavier ions) interact in intense photon fields during acceleration. Alternatively, it can be assumed that galactic sources are effective in producing particles through the knee region, but that the composition near 1 EeV (10^{18} eV) is at least partly due to cosmic rays of extragalactic origin. This independent source could have a composition very different from the low-energy composition. For example, the accelerated material could be primordial, consisting only of hydrogen and helium.

The energy region of interest in this article is near 1 EeV, well above energies at which the primary cosmic-ray composition has been measured directly. In this energy regime, the cosmic-ray composition is studied by observations of air showers, the cascades of billions of elementary particles produced when extremely energetic cosmic rays enter the atmosphere. As the cascade develops in the atmosphere, it grows until a maximum "size" (number of particles) is reached. The amount of air penetrated by the cascade when it reaches maximum size is denoted by X_{max}, with units of g cm^{-2}. For cascades of a given total energy E_0, heavier nuclei have smaller X_{max} because the shower is already subdivided into A nucleons when it enters the atmosphere. Evaluating X_{max} is a fundamental part of many of the composition studies done by observing air showers. Based on an analysis of the mean energy dependence of X_{max} from a variety of experiments, Linsley and Watson [14] concluded, for shower energies from 3×10^{16} to 10^{20} eV, that the combined assumptions of approximate Feynman scaling and rising hadron-air cross sections are in acceptable agreement with the data. Concerning the composition, they concluded that the mean $\langle \ln(A) \rangle$ has a 2σ upper limit of 1.1. This amounts to a significantly lighter composition than that obtained below the knee by JACEE.

Unlike other air shower experiments, the Fly's Eye [15,16] allows direct observations to be made of the development of cosmic-ray air showers. Thus both X_{max} and E_0 are primary observables, rather than parameters inferred from other measured quantities. The Fly's Eye detects the scintillation of the air from the very numerous $e^{\pm}$, $\mu^{\pm}$, and other shower particles. A weakly luminous track is detected and reconstructed, giving the trajectory of the primary cosmic-ray nucleus. In contrast with the shower's Cherenkov radiation, the scintillation light is emitted isotropically, allowing very remote detection of showers over areas of hundreds of square kilometers. The shower size (number of ionizing particles) is reconstructed from the intensity of scintillation light accounting for the atmospheric density and light absorption. In addition, the shower's total energy is evaluated from the total amount of ionization produced in the atmosphere.

The analysis of the composition proceeds by comparing the observed and expected X_{max} distributions for different assumed compositions. The nuclear physics models used in the Monte Carlo simulations are constrained by the available accelerator data. However, accelerator data in the laboratory are not available for extremely high energies and theoretical models must be used to predict the spectra of the secondary particles in the fragmentation region of the interaction which are important for the cascade development. The simulations show that there is significant overlap between the X_{max} distributions from such different primary nuclei as protons and Fe nuclei. The analysis must therefore accurately evaluate the biases produced in the accepted data due to detector triggering requirements and efficiencies in reconstructing the showers.

The Fly's Eye (FE) data used in the composition analysis will be described in Sec. II. The Monte Carlo simulations of showers and the detector efficiency will be covered in Sec. III. The results of the composition analysis are given in Sec. IV, followed by a discussion of these results and relevant quantities in Sec. V, and a presentation of the conclusions in Sec. VI.

II. DATA SET

The data set and the reconstruction methods used are similar to what is described in Cassiday *et al.* [17]. That paper discusses the data and analysis in terms of X_{max} distributions in some detail and should be referred to before proceeding with the present paper. As before, to ensure the most precise geometrical reconstruction, only data seen in stereo (i.e., simultaneously by both FEI and FEII) are used. The main difference is that here we have available a larger data set, which includes the original data (up to 1988 August) as well as subsequent data. This analysis is based on stereo data from November 1986 to June 1990, corresponding to a live time of 2649.1 h. There are three selection cuts applied to the data. The first, which requires that the estimated relative error in X_{max}, $\delta(X_{max})/X_{max}$, is less than 0.12, is the same as in the previous paper. This cut removes poorly reconstructed events. Note that the distribution of estimated errors in this variable is very similar for data and for the Monte Carlo events described below. For the second cut we now demand that the viewing angle between the shower axis and both FEI and FEII tubes be greater than 20 degrees, but only for the tubes that view the section of the shower at shower maximum (around X_{max}). This is less restrictive than the previous requirement that all viewing angles in an event be greater than or equal to 20 degrees, but it accomplishes the same purpose. This cut removes events with significant direct Cherenkov light contamination from the data sample, thus reducing the effect of systematic errors in the Cherenkov light subtraction algorithm. Finally there is an energy cut of greater than 0.3 EeV. This ensures that the data used are well above detector threshold. The total number of events passing all cuts in this sample is 2529.

Figures 5 and 7 below show the resulting elongation rate and shower maximum distribution as a function of energy. The elongation rate is defined as the logarithmic derivative of the mean depth of shower maximum [18,14]. It is sensitive both to properties of hadronic interactions (which determine the increasing penetration of higher energy showers) and to the primary composition (because light primaries penetrate more deeply than heavies of the

same total energy). This data set has a number of biases due to detector trigger, detector resolution, and data selection effects. These are discussed in detail in Cassiday *et al.* [17]. As before, we choose to account for them by generating simulated Monte Carlo events. The procedure is discussed in detail in Secs. III C and III D.

III. CALCULATION

The analysis of the Fly's Eye data, especially in terms of the cosmic-ray composition at ultrahigh energy, sets specific requirements on the simulation programs necessary to derive the desired results. On one hand, because of the extremely high energy of the primary nuclei, and correspondingly large number of shower particles ($\sim 10^9$ electrons at shower maximum for 10^{18} eV), the interaction model and the shower codes have to be fast enough to make the calculation feasible. On the other hand they have to give a good representation of the energy dependence of the inelastic interactions. In addition, the simulation should account for the biases introduced by the detection and analysis technique. We employ two different codes: (i) the shower Monte Carlo code that contains the high-energy physics input and generates the number of charged particles in individual showers as a function of the atmospheric depth and (ii) the detector Monte Carlo code, which simulates the triggering conditions and the detector response. We shall first describe the shower Monte Carlo code and its results.

A. Models of hadronic interactions

The heart of the shower Monte Carlo code is the hadronic interaction model. The main features of the hadronic interactions determine the behavior of the atmospheric cascades. Since there are no accelerator experiments that measure the interaction features relevant to the cascade development at the energies involved, it is important to illustrate the sensitivity of conclusions to the assumptions used in the interpretation of the measurements. Our approach in this paper is to use three models based on the same accelerator data, but which make rather different predictions for the extrapolation to Fly's Eye energies, equivalent to ~ 50 TeV in the c.m. system for nucleon-nucleon collisions.

Accelerator measurements for both proton and nuclear targets with proton, pion, and kaon beams are available up to several hundred GeV. In these experiments both fast and slow secondaries are detected. Collider experiments explore $\bar{p}p$ collisions in the region of phase space near $90°$ in the c.m. system (the central region) up to center-of-mass energy $\sqrt{s} = 1.8$ TeV, equivalent to a beam energy in the laboratory system of ~ 1 PeV. The fragmentation region of phase space (secondaries with energy larger than some fixed, small fraction ϵ of the beam energy) are not detected in the highest energy collider experiments. A well-known and striking result of the collider experiments is that the dimensionless phase space density of secondary particles in the central region increases with energy up to the highest accelerator energy

[19]. An essential question is how this scaling violation in the central region affects the fragmentation region of the high-energy interactions, which is important for the development of cosmic-ray cascades. An added theoretical complication is the transition from proton-proton interactions to proton-nucleus and nucleus-nucleus interactions, which has to reflect the basic physics of the models. In summary, we need models that relate central region to fragmentation region, relate proton-proton interactions to hadron-nucleus and nucleus-nucleus interactions, and support extrapolation by 1.5 orders of magnitude in c.m. energy beyond the most energetic collider.

We have chosen [20–23] three representative models of high-energy inelastic interactions, which are characterized by different predictions for the energy dependence of a key quantity, the *inelasticity*. We define the inelasticity in the laboratory system as the fraction of the energy of an incident particle that is not carried out of the interaction by the fragment of the incident particle (i.e., by a fast proton or neutron in the case of an incident proton).[1] If x_{ldng} is the fraction of the energy carried by the leading fragment,

$$K_{\mathrm{inel}} = 1 - x_{\mathrm{ldng}}. \tag{1}$$

The inelasticity is also often defined in the center-of-mass system as

$$K_{\mathrm{c.m.}} = 1 - \tfrac{1}{2}(x_1 + x_2), \tag{2}$$

where $x_i = 2E/\sqrt{s}$ is the fractional energy of the leading fragment in the ith hemisphere. For pp collisions it is easy to show that $\langle K_{\mathrm{c.m.}} \rangle = \langle K_{\mathrm{inel}} \rangle$, though the distributions of inelasticity are in general different in the two coordinate systems. Physically, the inelasticity is the fraction of energy available for particle production. Shabelski *et al.* [24] give a useful discussion of inelasticity in various models.

Each of the models we use relates the inelasticity to the energy dependence of the central region in a different way.

1. Statistical model

Versions of this model, which are related to the Landau [25] hydrodynamical model, have been widely used in cosmic-ray cascade calculations [26–29]. Its main feature is that the multiplicity is proportional to a power of the available center-of-mass energy. $\langle n \rangle = \mathrm{const} \times (K_{\mathrm{inel}}\sqrt{s})^\alpha$. To match the observed rise of the rapidity density from $\sqrt{s} = 53$–1800 GeV, the power-law increase of the multiplicity must be compensated for [28] by a decrease in K_{inel}. At $\sqrt{s}$ of 540 GeV K_{inel} has to be decreased to 0.3 from the canonical low-energy value of 0.5. A further decrease to 0.2 is necessary to explain the multiplicity at $\sqrt{s}$ of 1.8 TeV. The effective value of α in our version is 1/3.

---

[1]Ambiguities arise in the experimental definition of inelasticity due to the production of particles indistinguishable from beam fragments. Normally, these are of low energy and therefore not a serious problem.

2. Kopeliovich-Nikolaev-Potashnikova (KNP) model

This model [30] uses the language of the QCD Pomeron [31]. It relates the increase of the cross section to an increase of particle production in the central region and to an increase with energy of inelasticity. The inelasticity increases relatively rapidly with energy because of a "leading particle cascade" assumption [32]. The model for proton-proton collisions has a multiple scattering framework, reminiscent of Glauber theory [33] for nuclear collisions. The average fractional leading nucleon energy with n cut Pomeron exchanges is given by a recurrence relation to the single cut Pomeron case. Thus $\langle x \rangle_n = (\langle x \rangle_1)^n$. This gives a rapid decrease with x of the leading nucleon spectrum and a correspondingly strong increase of K_{inel}. This model can be considered to give an upper bound to the rate of increase of inelasticity.

3. Minijet model

This model relates the increase of the cross section to interactions between soft constituents (gluons and sea quarks) of the incident hadrons [34–38]. These constituent interactions produce soft jets, which become more numerous as energy increases, leaving less energy for the beam fragments. Although the number of jets increases with energy, the fractional energy of each jet decreases. Thus the inelasticity increases only slowly with energy in this model even though the jet production accounts for the increasing multiplicity and strong scaling violation in the central region [39].

4. Nuclear effects

One can use Glauber's multiple scattering theory to calculate the inelastic cross section for hadron-nucleus interactions as discussed by Anisovich et al. [40]:

$$\sigma_{\text{inel}}^{hA}(s) = 2\pi \int b \, db (1 - e^{-\sigma_{\text{inel}}^{hh}(s)T(b)}) \qquad (3)$$

where $T(b)$ is the nuclear profile. $\sigma_{\text{inel}}^{hA}(s)$ can be expressed as a sum of cross sections for having ν wounded nucleons in the target with the average number of wounded nucleons $\langle \nu \rangle = A\sigma_{\text{inel}}^{hh}/\sigma_{\text{inel}}^{hA}$. Since we use in our calculation the same form of σ^{pp} that fits the collider results, we end up with the same wounded nucleon distributions for all three models. The difference is in the treatment of the beam interactions inside the target.

In the KNP model, p-nucleus interactions are treated in the same way as multiple Pomeron exchanges in p-p scattering: nuclear target effects are a consequence of the reinteraction of the beam. Accordingly, in terms of the wounded nucleon probability P_ν,

$$\langle x_{\text{ldng}} \rangle^{pA} = \sum_{\nu=1}^{A} P_\nu (\langle x_{\text{ldng}} \rangle^{pp})^\nu . \qquad (4)$$

The beauty of this model is that there is actually only one parameter, the pp cross section, that determines all properties of the interaction, and the scaling violation

and cross section are strongly correlated. We have used the same approach to implement the nuclear target effects in the statistical model, i.e., for $\nu > 1$ the subsequent incident nucleon interactions were treated analogously to the first one. This treatment leads to an increase of the effective α value to 0.44. The results for p-nucleus interactions we obtained from our version of the statistical model are very close to the examples given by Wilk [41].

For the minijet model we implemented the scheme of the dual topological unitarization model of Capella and Tran Thanh Van [42]. While the p-nucleus interactions for $\nu=1$ are the same as pp interactions, subsequent beam collisions involve sea-quark pairs, associated with the beam. Since the structure functions of sea quarks are softer than these of valence quarks, the beam loses less energy in these additional collisions. Then x_{ldng} can be calculated as

$$\langle x \rangle^{pA} = \langle x \rangle^{pp} \left[1 - \sum_{\nu=2}^{A} P_\nu \langle x_{\text{sea}}(2(\nu-1)) \rangle \right], \qquad (5)$$

where $\langle x_{\text{sea}}(2(\nu-1)) \rangle$ is the total fractional energy carried by the interacting sea quarks in the projectile.

Nuclear interactions of pions and kaons were treated in an analoguous way, using the appropriate meson cross sections on protons and nuclei. The method we use here is more accurate than models of hadron-nucleus collisions in which hadron-nucleon models are scaled to the
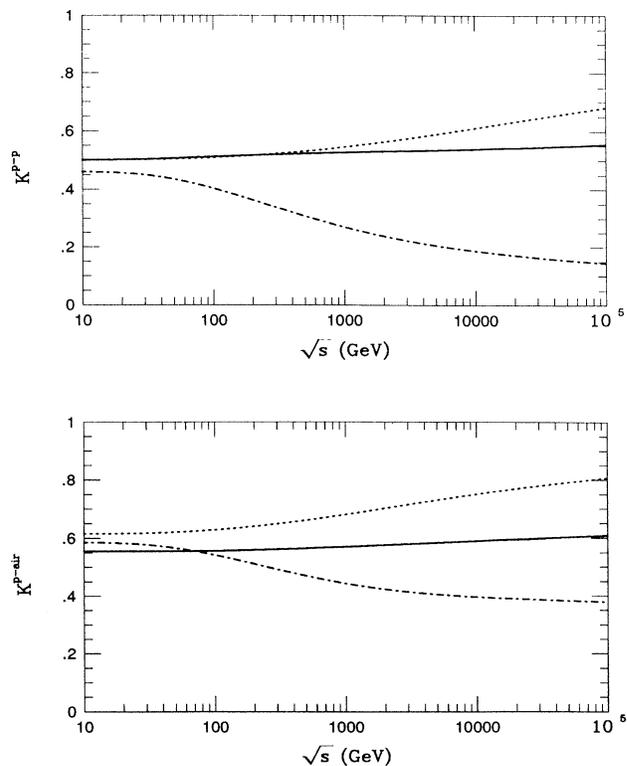

FIG. 1. Inelasticity for the three models discussed in the text. Upper panel is for pp and lower panel for p-air collisions. In each case the highest line is KNP, the middle line is minijet, and the lower line is statistical model.

p-nucleus according to experimental results at low energy [43]. The present model accounts for the rise of the hadron-nucleon cross sections, so that nuclear target effects become more pronounced at very high energy.

The dependence of inelasticity on energy in the three models is shown in Fig. 1 both for proton-proton and for proton-nucleus collisions. Inelasticity for interactions of pions and kaons has a similar energy dependence. For the purposes of this analysis, all three models were coded in a simplified way [22]. For each event the momentum of the leading particle is sampled from a distribution of the form $x\,dn/dx = \mu x^{\mu}$, as suggested by KNP, with μ adjusted for each model to give the desired inelasticity. The energy remaining after the beam fragment is selected must then be used for production of secondary mesons. For this purpose we use the splitting algorithm of Hillas [44] with an energy-dependent number of presplittings adjusted to give the same multiplicity of particles in the central region in all three models. In the minijet algorithm, the energy removed from a nucleon in secondary interactions inside the nucleus was sampled using appropriate sea-quark structure functions. In all three models, K_{inel} is larger for nuclear targets than for protons.

Both KNP and minijet models show only a slight scaling violation for pion distributions in the fragmentation region. In contrast, in the statistical model the inclusive distribution for pions becomes much softer as energy increases, as the energy carried off by the leading nucleon increases.

The collisions of heavy nuclei with air were modeled using the "semisuperposition" model of Engel et al. [45]. As in the superposition model, each "wounded nucleon" in the projectile is assumed to generate a nucleon-air interaction. Unlike the superposition model, however, this model accounts in a realistic way for fluctuations in the number of wounded nucleons in the projectile nucleus, as well as fluctuations in the fragmentation of the residual nucleus into "spectator" nucleons and nuclear fragments. As a consequence there are strong correlations among the depths of the first interaction of the nucleons of a primary nucleus, which induce large fluctuations in the position of X$_{\text{max}}$ even for showers generated by heavy nuclei.

B. Results from the shower Monte Carlo code

The calculation is performed by following directly the interactions of all shower particles down to 1/300 of the primary energy per nucleon. Parametrizations based on calculations with a lower primary energy with the corresponding interaction models were used to calculate the contributions to the shower size by subthreshold hadrons. γ rays from decay of neutral particles with energy above threshold were followed in a direct Monte Carlo fashion, while subthreshold electrons and photons were fed into Greisen's [46] formula, which has been proven to describe quite well the longitudinal development of electromagnetic showers. For both types of subthreshold particles a method developed by Gaisser [47] was used to sample individual shower profiles from a known average shower behavior.

The resulting hybrid program is still not free of biases.

The use of Greisen's approximation in combination with the electromagnetic Monte Carlo part leads to systematic shifts of the order of 10 g/cm^2 in the calculated depth of maximum. The Monte Carlo part of the electromagnetic code is however essential for a correct representation of the fluctuations in the shower development. The systematic shift has been investigated and shown not to be energy dependent. We then used the described scheme with the idea of accounting for the systematic shift at the final stage of the analysis.

To investigate the dependence of the major shower parameters on the interaction model we calculated sets of showers with fixed primary energy above 10^{16} eV for each of the three models. The results of the KNP and the minijet models are quite similar, while the statistical model predicts, as expected, more penetrating showers. The elongation rates for proton showers of energy between 10^{16} and 10^{19} eV are, respectively, 60 ± 2, 55 ± 1, and 52 ± 2 g/cm^2 for the statistical, minijet, and KNP models. The average depths of shower maximum $\langle X_{\text{max}}\rangle$ at proton energy of 1.25×10^{18} eV are, respectively, 807 ± 6, 775 ± 4, and 762 ± 4 g/cm^2. (Depths are measured along the shower trajectory.) These are values that come directly from shower Monte Carlo calculations and cannot be compared to experimental data without accounting for the detector efficiency and detection biases.

We also simulated a set of showers with energy distribution following that measured by Fly's Eye [17] for three types of primary nuclei: H, CNO, and Fe, in order to study the influence of the models on showers generated by heavier nuclei. The average depths of maximum are presented in Table I. Although the differences between interaction models are not insignificant, the primary nuclei introduce significantly bigger changes in X_{max}. The biggest model difference is for proton showers in the KNP and statistical models: 39 g/cm^2. In contrast, proton and Fe showers have X_{max} differing by ~ 100 g/cm^2 in all models. The model dependence for heavier nuclei is slightly smaller than for protons. Figure 2 shows the X_{max} distributions for proton showers in all three models. The showers calculated with the statistical model develop quite deep in the atmosphere and show a noticeable number of showers having X_{max} greater than 1000 g/cm^2. This is at least partly a consequence of the fact that we use the same, relatively slowly increasing cross section for the statistical model calculations as for the

TABLE I. Mean X_{max} for three models and primary nuclei.

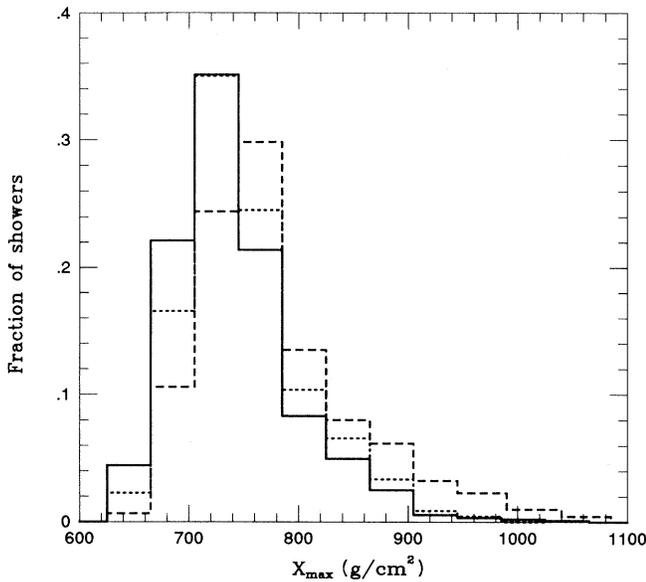|	H	CNO	Fe
KNP	750±1.9	711±0.9	653±0.8
Minijet	761±1.9	719±1.0	663±0.8
Statistical	789±2.4	744±1.1	681±0.8

FIG. 2. Depth of maximum distribution for proton showers, simulated by the shower Monte Carlo calculations with energy spectrum as in Cassiday *et al.* (1990). Showers simulated with the KNP model are plotted with a solid line, minijet model—dotted line; statistical model—dashed line.

other models. (This cross section is discussed and plotted as the solid line in Fig. 9.) Wilk and Wlodarczyk [29] combine decreasing inelasticity with a more rapidly increasing cross section than we use to generate more rapidly developing showers in a statistical model.

C. Detector Monte Carlo program

In order to make the calculated showers comparable to the experimental data, we use a detector Monte Carlo program which takes into account the triggering efficiency and reconstruction resolution of the detectors. The input for the detector Monte Carlo program are the files calculated by the shower Monte Carlo code, which contain individual shower profiles with energies sampled from an E^{-3} differential energy spectrum. Each of these showers is assigned a random direction, zenith angle, and impact distance to the Fly's Eye. The amount of light is calculated as a function of the atmospheric depth as a sum of the nitrogen fluorescence and direct and scattered Cherenkov radiation. Solid angle effects and light extinction due to atmospheric Rayleigh and aerosol scattering are then taken into account, and the amount of light arriving at each individual mirror is calculated. The optical and electronic characteristics of the detectors are then modeled to produce the output consisting of a list of firing photomultipliers with associated timing and amplitude information. This output is finally analyzed with the standard analysis algorithms [17], producing a sample of simulated events corrected for the triggering efficiency, acceptance, and reconstruction resolution of the detector.

We have investigated the systematic errors that might be present in the analysis [17]. These are (a) variations in

aerosol differential scattering cross sections and aerosol density as a function of altitude from the standard atmospheric model, (b) summer/winter atmospheric pressure profile variations at the location of the experiment (Dugway Proving Grounds), and (c) the model dependence of the residual direct and scattered Cherenkov radiation in a shower. For the case of atmospheric extinction and Cherenkov light subtraction the parameter values chosen in the models are actually minimum values. Increasing these by the estimated error in the parameter in the reconstruction algorithm systematically moves the simulated showers to shallower depths in the atmosphere. These sources of systematic errors can individually generate shifts in X_{max} of not more than 10 g/cm^2. Since these systematic shifts are independent, the different sources of systematic errors can add up. We estimate that the simulated showers can be shifted to shallower X_{max} to a maximum of about 20 g/cm^2, or alternatively the experimentally detected showers can be assigned X_{max} deeper by the same amount.

D. Detector biases

In addition to the systematic shifts discussed above which can result in a relative shift between simulated and real data, there are shifts due to detector and reconstruction biases between the true and reconstructed distributions. These affect the data and the simulated events in the same way. To analyze the biases introduced by the separate stages of the detector Monte Carlo code we first simulated sets of showers at fixed energy and calculated the important parameters after every step. Here is a typical result from simulation of 1-EeV proton showers with the KNP interaction model where both parameters are in g/cm^2:
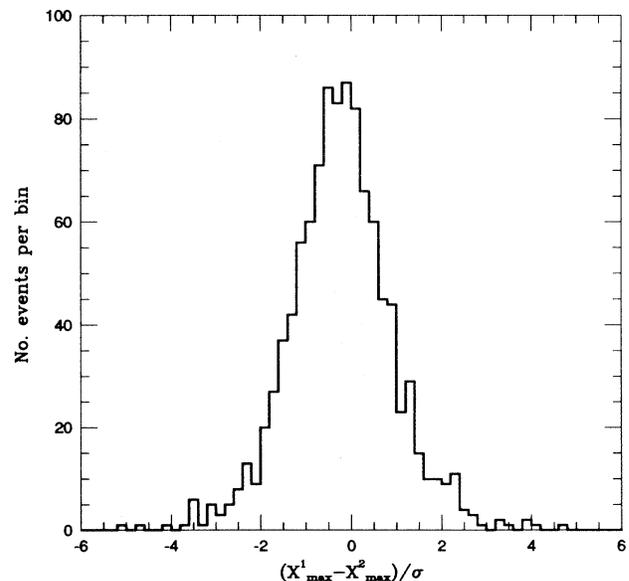

FIG. 3. Distribution of the difference between X_{max} assigned to experimental showers reconstructed separately by FEI and FEII.

Input from the shower Monte Carlo code: $\langle X_{\max}\rangle$=755±2; $\sigma_{X_{\max}}$ =56±1.
After triggering: $\langle X_{\max}\rangle$=751±2; $\sigma_{X_{\max}}$=47±2.
After reconstruction: $\langle X_{\max}\rangle$=769±4; $\sigma_{X_{\max}}$=83±3.
Final, after cuts: $\langle X_{\max}\rangle$=768±5; $\sigma_{X_{\max}}$65±0.4.

The final result after the whole procedure shows that the average shift for KNP and minijet proton showers is ~11–13 g/cm². The width of the distribution increases more significantly, by about 16–18%. The effect is stronger for showers generated by heavier nuclei, which are characterized by shallower $X_{\max}$ and smaller $X_{\max}$ width. The final shifts for 1-EeV-iron showers is from $\langle X_{\max}\rangle$=656±0.5 to 678±3.4 g/cm² and from $\sigma_{X_{\max}}$=38±0.2 to 53.6±1.5 g/cm².

The increase in width is consistent with folding in the Monte Carlo estimated detector resolution of 45 g/cm². Note that this estimated resolution can be directly measured by comparing $X_{\max}$ measured by FEI and FEII on an event-by-event basis. Figure 3 shows the resultant distribution in the variable $(X_{\max-1} - X_{\max-2})/[\sigma(X_{\max-1})^2 + \sigma(X_{\max-2})^2]^{1/2}$. The resolution is approximately Gaussian with a mean σ of 47.3 g/cm², in good agreement with the Monte Carlo estimate.

The biggest contribution to the $X_{\max}$ shift, comes from poorly fitted showers, which are assigned too deep a depth of maximum. The situation is illustrated in Fig. 4 where the $X_{\max}$ distributions of Fe showers with energies between 1 and 3 EeV, simulated with the KNP model, are plotted before and after the treatment with the detector Monte Carlo code. The shift of the average $X_{\max}$ is +24 g/cm² and width of the distribution is increased by 16 g/cm². Fe showers are thus shifted by an additional 10 g/cm² more than proton showers. The faster shower development makes Fe showers more distant from the de-
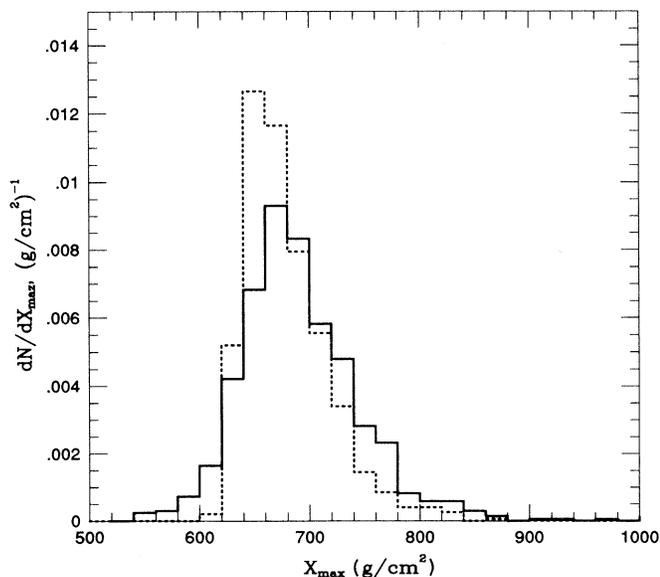

FIG. 4. Depth of maximum distribution of Fe showers of primary energy between 1 and 3 EeV before (line) and after (shaded area) accounting for the detector resolution with the detector Monte Carlo code.

tector than proton showers. The shower track length in the detector is thus smaller and the light absorption more significant. Both effects lead to a less precise reconstruction. However, since this is a reconstruction effect we expect the real data will be shifted by the same amount as the simulated data.

Several production runs were made with both Monte Carlo programs. Showers generated by the three types of primary nuclei with an E^{-3} differential energy spectrum were simulated and sets of Monte Carlo "detected" showers were collected. The statistics of every run is about three times bigger than the current experimental sample. Table II contains the averages and widths of these samples. Only the KNP and the minijet models were used in the production runs because our version of the statistical model produces very late developing showers, which do not match the experimental data.

IV. COMPOSITION

The last and most important step of our analysis is the comparison of the Monte Carlo simulated events with experimental data and fitting the data with different composition models. As stated above we estimate a systematic shift of the Monte Carlo events sample of 10 g/cm² and a possible systematic shift of the experimental data of not more than 20 g/cm². We fit the experimental data by shifting the Monte Carlo events to shallower $X_{\max}$ by 25 g/cm² and not manipulating the experimental data set. A smaller shift and no shift at all does not change our qualitative conclusions on the composition of cosmic rays.

Figure 5 shows the depth of maximum versus primary energy for the experimental sample compared with the Monte Carlo predictions for Fe (lower band) and H (upper band). The width of the bands shows the systematic and statistical errors of the simulation. To construct the bands we have taken the lower statistical error (shallow $X_{\max}$) for the KNP model, which predicts slightly faster shower development to represent the minimum $X_{\max}$ value, and correspondingly the upper error of the minijet model to represent the maximum $X_{\max}$ value of the Monte Carlo predictions. Because of the fluctuations in the number of events per bin the widths of the bands are not constant.

It is obvious from Fig. 5 that both versions of the Monte Carlo predictions predict slower energy dependence of $X_{\max}$ than the data shows. The measured elongation rate L_E [$=dX_{\max}/d(\log_{10}E)$] is 75.3 ± 4.0 g/cm². This is to be compared with the value inferred by Walker and Watson [48] of 70±5 g/cm² averaged over their whole energy range from 0.2 to 100 EeV. Kifune [49] has made a summary of various measurements of shower depth of maximum versus energy (including Fly's Eye data). The range of $X_{\max}$ from different experiments is about 50 g/cm² at any given energy. The trend of the data sum-

TABLE II. Results from the detector Monte Carlo program.

	KNP			Minijet		
	Number	$\langle X_{max} \rangle$	σ	Number	$\langle X_{max} \rangle$	σ
H	4894	764.7	60.0	4890	748.4	64.7
CNO	5249	701.5	54.0	5150	710.6	54.2
Fe	5289	668.3	50.9	5261	681.3	51.0

mary between 0.1 and 10 EeV can be fit with a straight line with slope $\sim$ 70 g/cm^2. Thus all the measured elongation rates are consistent with each other, within rather large uncertainties. In contrast, both Monte Carlo models predict L_E of 49 $\pm$ 3 g/cm^2.

In addition, we are not able to fit the whole sample with a unique compostion. In further analysis, we therefore divide the data into three energy groups: 0.3–0.5, 0.5–1.0, and > 1 EeV with approximately equal statistics. We fit a composition in each range separately, using a χ^2 minimization procedure.

Although the calculations were done for H, CNO, and Fe nuclei, and we refer to the fits in the same way, these nuclei have to be viewed as representing much broader groups of nuclei. Our simulations in the past [43] have shown that H and He nuclei are not distinguishable by the Fly's Eye. Similarly, what we call Fe includes all nuclei heavier than the CNO group. When we perform a three-parameter fit, the fitting program tends to neglect

the CNO fraction of the composition. Table III lists the fractions of H and Fe with their errors, as well as the normalized χ^2_{min} for 22 degrees of freedom. The fit quality in the lowest energy bin is not very good, possibly because of poorer reconstruction close to the detector threshold. The large χ^2 values are, however, due to a small number of experimental showers (see Figs. 7 and 8) having X_{max} shallower than the simulated Fe events, which cannot change the conclusion that the cosmic-ray composition in this energy range appears to be very rich in heavy elements. Figure 6 shows the χ^2 contour plot in the H and Fe fraction space for our best fit – KNP model for E >1 EeV. The dot shows the most probable value of these fractions. The corresponding fraction of CNO nuclei is 0.01. The fitting routine needs to preserve the Fe component to match the rising edge of the X_{max} distribution and the H component to match the tail of the distribution. However, if we fix the fraction of iron at a suitable value, we get a three-component fit with almost as good a χ^2 as the two-component fit. For example, for the case E > 1.0 EeV and the KNP model,
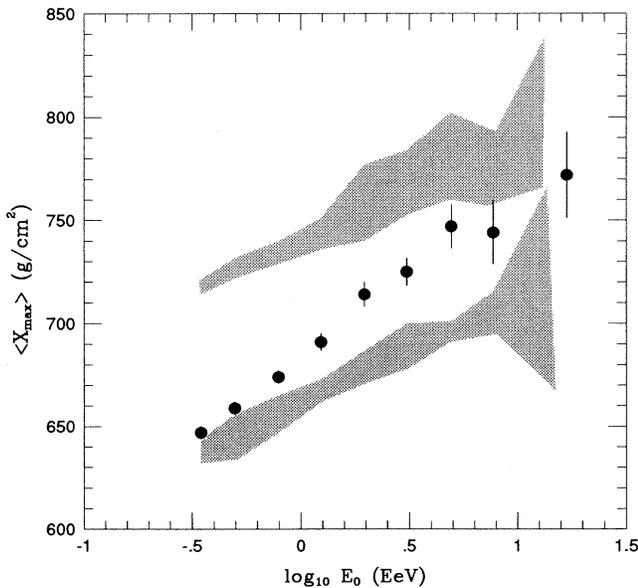

FIG. 5. X_{max} dependence on the primary energy for the experimental set of showers (data points) compared to the Monte Carlo results for H (upper band) and Fe (lower band) showers. The Monte Carlo bands include both statistical and systematic errors.
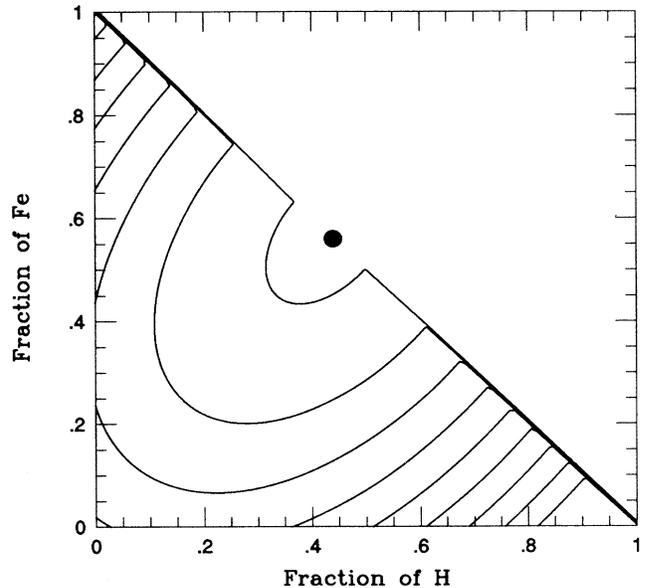

FIG. 6. χ^2 contour plot of the fit of the X_{max} distribution of showers with energy above 1 EeV with the KNP model. Contours are for normalized χ^2 = 1, 2, 3, etc.

TABLE III. Results from the composition fit.

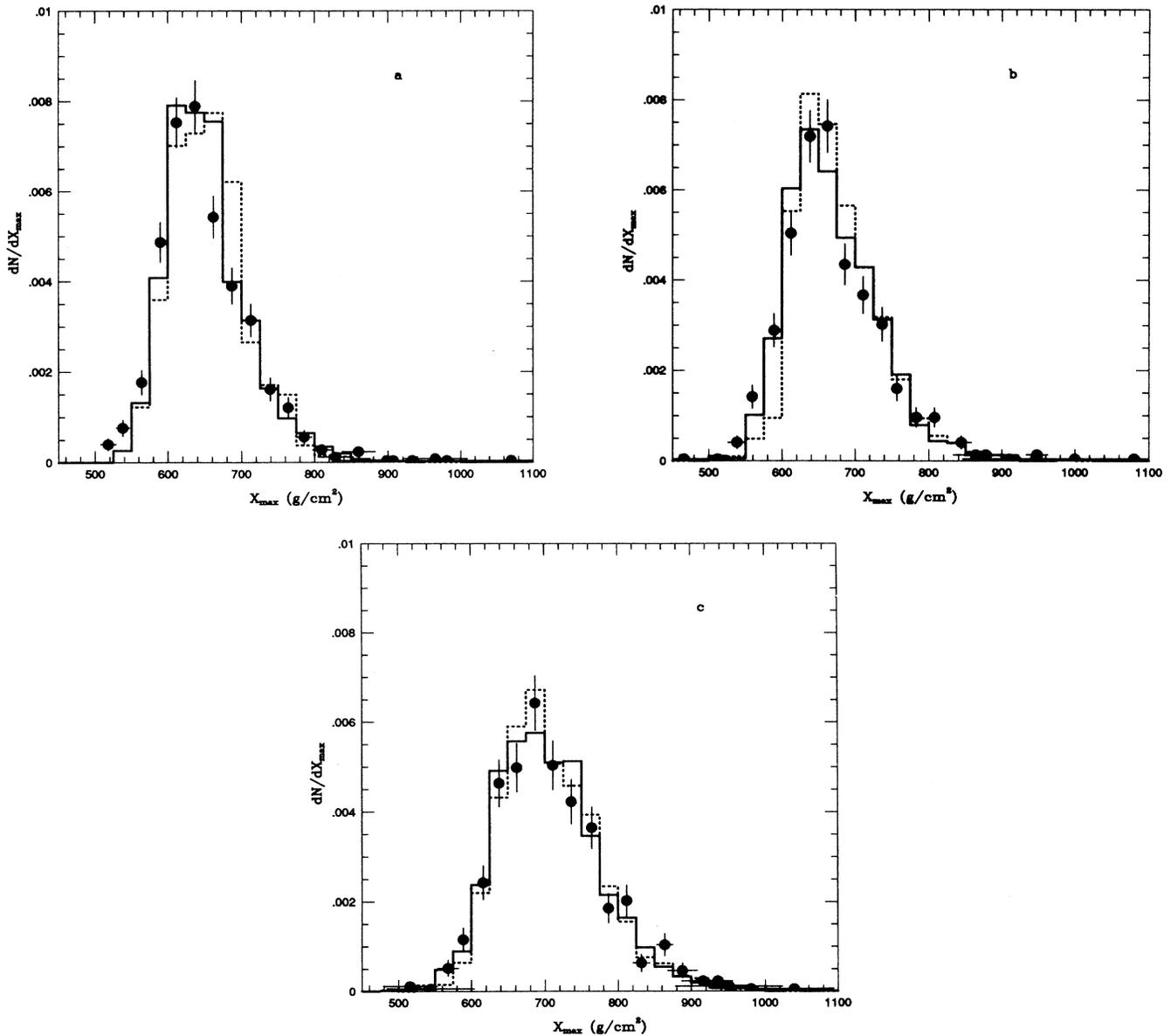| E, (EeV)	Number	KNP model			Minijet model		
		H	Fe	χ^2	H	Fe	χ^2
0.3–0.5	994	0.21±0.07	0.79±0.11	2.51	0.12±0.03	0.88±0.06	4.85
0.5–1.0	867	0.27±0.12	0.66±0.12	1.56	0.21±0.10	0.79±0.16	3.17
> 1.0	690	0.43±0.04	0.56±0.05	0.96	0.39±0.15	0.61±0.17	1.32

FIG. 7. Comparison of the experimental X_{max} distribution (number of showers per g/cm^2) with the fitted Monte Carlo distributions for (a) 0.3< E <0.5 EeV, (b) 0.5< E <1 EeV; and (c) E > 1 EeV. Solid histograms—KNP model; dotted histograms—minijet model.

fixing the Fe contribution at 40% and allowing the CNO and p contributions to vary, leads to a χ^2 minimum near 20% CNO and 40% protons. This corresponds to a χ^2 of 26.2 for 22 degrees of freedom, which is only marginally larger than the best two-component fit. A satisfactory three-component fit can only be obtained for an Fe concentration between 30% and 50%. It seems clear that the present data are not very sensitive to the CNO component but can easily accommodate its presence at the 20% level. It is interesting that the JACEE composition quoted in the Introduction, when reclassified into three groups of nuclei, gives 36% Fe, 26% CNO, and 37% pro-

tons. Using these numbers leads to a χ^2 fit to the data of 32.7, still a reasonable fit for 22 degrees of freedom. By contrast, a pure H composition leads to a χ^2 of 288. We return to this point below in connection with our discussion of energy dependence of the cross section, where we find that fits with a somewhat smaller proton cross section would require a reasonable fraction of intermediate nuclei.

Figure 7 shows the X_{max} distributions in the three energy intervals and the fits with the compositions of Table III. Figure 8 shows the same on a logarithmic scale so that both the rising edge and the tail of the distribu-
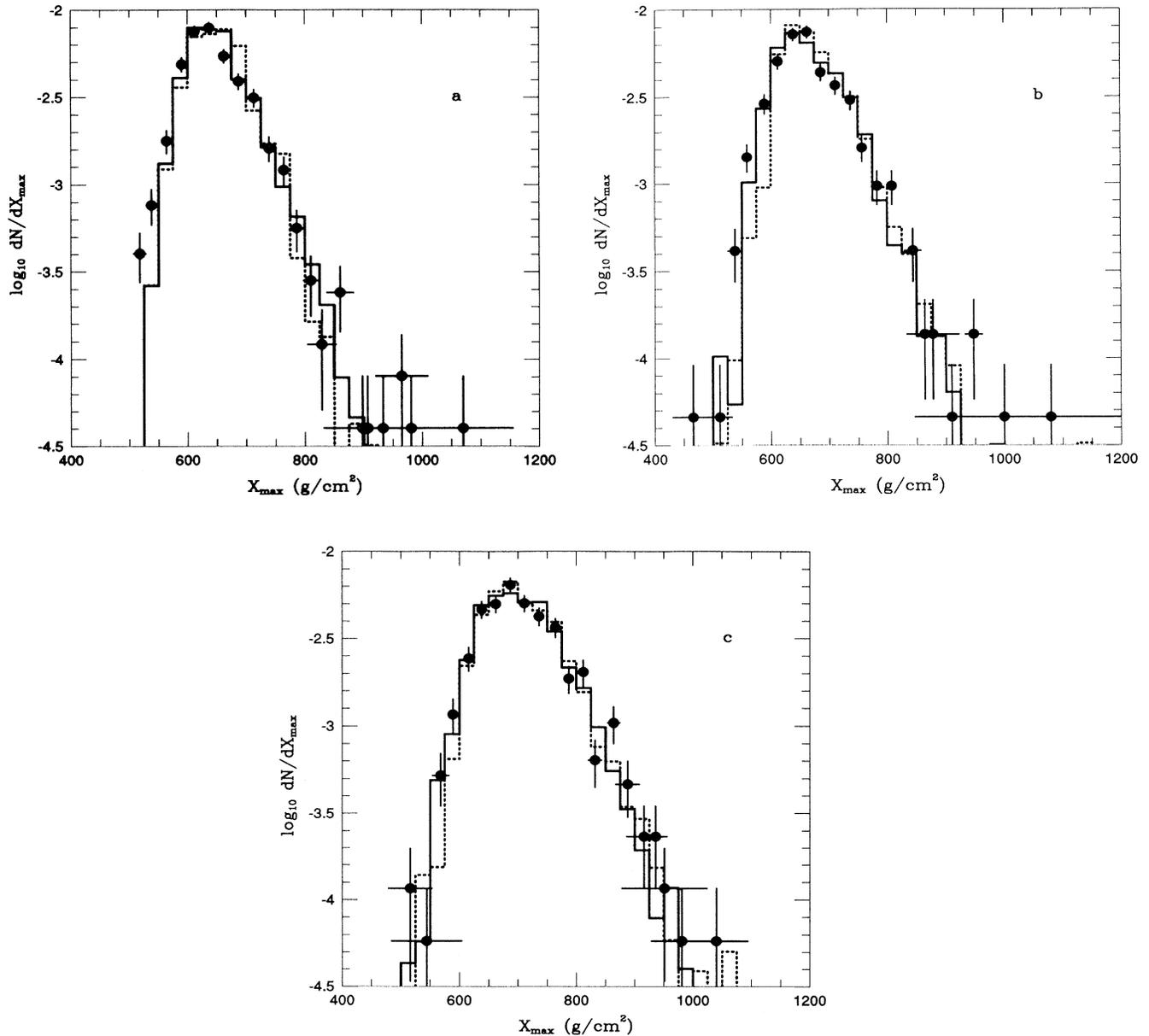

FIG. 8. Same as Fig. 7 plotted on a logarithmic scale.

tions can be better examined. Smaller shifts between simulated showers and data increase the proportion of Fe required but they also decrease the goodness of fit of the simulations to the data.

V. CROSS SECTION

In this section we consider the effect of different choices for the energy dependence of σ_{p-air}^{inel} on the X_{max} distribution of protons. Since, for the case of the minijet and KNP models, this energy dependence is a consequence of the physics, choosing a different energy dependence is an artificial, but still useful exercise, since it shows the sensitivity of the X_{max} distribution to this variable. In what we describe below, the minijet model inelasticity and multiplicity are used, and we try four different energy dependences for σ_{p-air}^{inel}. (These are the same dependences used in the previous Fly's Eye paper on this subject, Baltrusaitis et al. [50].) They are (i) constant cross section, (ii) $\ln(s)$, (iii) $\ln^2(s)$, and (iv) the Leader-Maor (LM) model [51] which has an extreme increase with energy. Figure 9 shows the resulting energy dependences and normalizations.

As is discussed in detail by Ellsworth et al. [43], the main expected effect of changing σ_{p-air}^{inel} is a change in the decrement or falling slope of the proton X_{max} distribution. If this slope is characterized by an exponential, the exponential slope λ is related to the proton interaction length. In our previous work, the effect of energy and X_{max} resolution and trigger efficiency on this relation was only roughly accounted for. Here we use our full Monte Carlo simulation set to examine this question.

Because we are particularly interested in the decrement

TABLE IV. Dependence of proton X_{max} decrement and $\langle x_{max} \rangle$ on σ_{p-air}^{inel} energy dependence.

Model	$\langle X_{max} \rangle$	λ
CNST	823 ± 2.2	83.3 ± 7
ln(s)	769.8 ± 1.0	55.5 ± 3
Minijet	766 ± 1.4	55.6 ± 3
KNP	760 ± 1.3	55.5 ± 5
$\ln^2(s)$	750.7 ± 1	43.4 ± 6
LM	706.0 ± 1.5	35.7 ± 3
Data		62.5 ± 4

λ we are concerned about poorly measured events which are typically reconstructed deep in the atmosphere. To reduce this effect we use a tighter set of cuts than what was used to study the composition. They are, relative error in X_{max}: < 0.08; viewing angle near X_{max}: > 25 degrees and $E > 0.56$ EeV. Figure 10 shows the X_{max} distribution for simulated protons with the four different energy dependences. An exponential fit for $X_{max} > X_{peak} + 100$ g/cm^2 where X_{peak} is the location of the maximum of the X_{max} distribution yields the results shown in Table IV. This table also includes the results for the KNP and minijet models discussed previously. Note that changing the σ_{p-air}^{inel} energy dependence also changes the mean X_{max} of the proton distribution.

Since the data include a significant amount of heavy nuclei, their effect on the decrement (as defined above) must be estimated. We do this for the case of the minijet and KNP models by fitting the decrement for the best two-component composition fit using the tighter cuts defined above. The resultant decrement changes by ~ 5
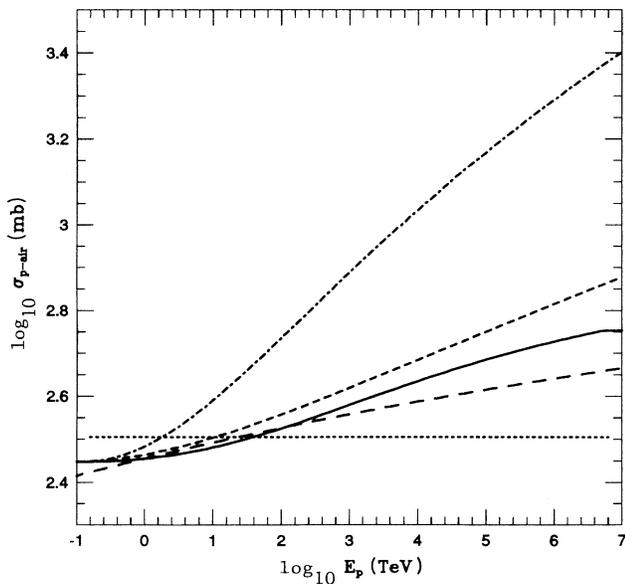

FIG. 9. Energy dependence of different cross-section models. The solid line shows the cross section used in the composition calculation; dots—constant cross section; long dashes—ln(s) energy dependence; short dashes—ln^2(s) energy dependence; dash-dots—LM model.
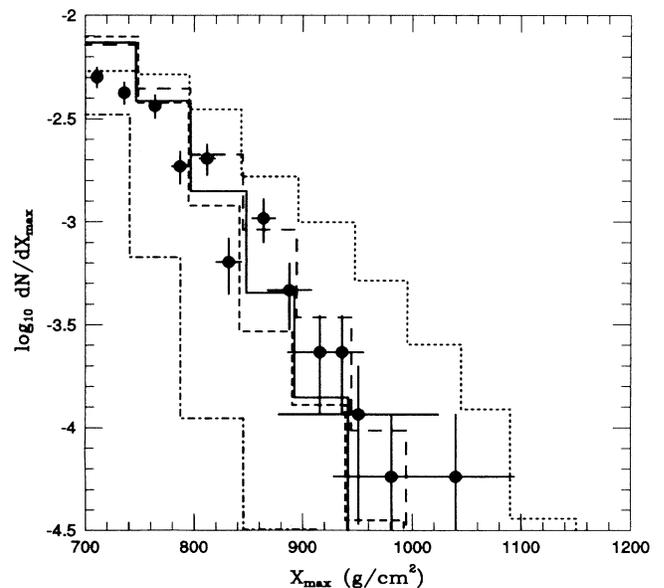

FIG. 10. X_{max} distributions for simulated proton showers with different proton-air inelastic cross sections compared to the tail of the experimental distribution. All showers are with energy above 1 EeV. The cross sections are coded as in Fig. 9.

g/cm^2 from the pure proton result. This is then a measure of the systematic error on the decrement due to the presence of heavy nuclei in the data.

We note the following.

(a) The decrement of the data is consistent with both minijet, minijet + ln(s), and KNP energy dependences and strongly inconsistent with a constant or LM model dependence. This conclusion applies to the sum of the inelastic nondiffractive, double diffractive, and a half of the diffractive cross section, since the shower development is not affected by backward diffractive interactions.

(b) A purely protonic composition cannot be rescued by increasing the $\sigma_{p-\text{air}}^{\text{inel}}$ cross section. Although the proton distribution will then have a mean X_{max} similar to the data, the proton decrement will be significantly smaller than the measured value.

(c) At the other extreme, a constant cross section produces such deep proton showers that only a very small fraction of the observed X_{max} distribution can be accounted for. The resultant composition would have to be extremely heavy.

Because of statistical limitations, we have only been able to look at the decrement integrated over the energy range 0.56–10 EeV. Increased statistics, such as will be available with the high-resolution Fly's Eye experiment, will allow us to fit separately the decrement in different energy bins and arrive at the energy dependence in a much more direct manner.

VI. DISCUSSION

Comparison of the X_{max} distribution of the data with three hadronic models and Fe and H incident nuclei leads to the following conclusions.

(a) Our version of the statistical model (with relatively slowly increasing inelastic cross section shown by the solid line in Fig. 9) does not fit the data for any choice of composition.

(b) Both the KNP and minijet models require a substantial flux of Fe to account properly for the observed rise of the X_{max} distribution. A substantial flux of H nuclei is also required to account for the tail of the distribution. Although the exact proportions of heavy nuclei and H vary, the conclusion that we are observing a mixed composition is independent of choice of KNP or minijet models.

(c) A light composition cannot be rescued by using an extreme energy dependence for $\sigma_{p-\text{air}}^{\text{inel}}$ since this leads to a decrement much smaller than is observed. We have not, however, explored the possibility of simultaneously decreasing the inelasticity and increasing the cross section, as advocated by Wilk and Wlodarczyk [29]. Extrapolations of conventional fits to accelerator data do not favor a rapid increase of $\sigma_{p-\text{air}}^{\text{inel}}$. For example, Block, Halzen, and Margolis [52] predict σ_{pp}^{tot} between 118 and 135 mb at $\sqrt{s}$ = 40 TeV, using three different parametrizations normalized to accelerator data up to $\sqrt{s}$ = 1.8 TeV.

(d) The observed decrement is consistent with a near ln(s) energy dependence for the inelastic cross section (long dashes in Figs. 9 and 10), which is consistent with

the assumed energy dependence of the KNP and minijet models, as shown by the solid line in the figures.

(e) If the extrapolations of Block, Halzen, and Margolis [52] are converted [53] to p-air cross section using the Chou-Yang [54] relation between slope parameter and pp cross section, one finds values for $\sigma_{p-\text{air}}^{\text{inel}}$ that lie between the solid line and the ln s extrapolation in Fig. 9. Use of a smaller proton-air cross section will have the effect of shifting the depth of maximum of proton showers down in the atmosphere relative to showers generated by nuclei, leaving room in the middle of the depth of maximum distribution for showers generated by heavy nuclei. This effect has been studied artificially by shifting the protons deeper by 10 g/cm^2 and refitting the three-component composition. The best fit then requires a 10–20% fraction of CNO component in each energy bin.

(f) Both the comparison of the elongation rate with models (Fig. 5) and the detailed comparisons of X_{max} distribution in three energy bins (Table III) suggest an increasing fraction of protons (and/or helium) with energy. One should bear in mind, however, that this conclusion depends entirely on the comparison of the data with the models. A constant composition would require a hadronic model with a significantly greater elongation rate than we have with the present models.

(g) The elongation rate for pure Feynman scaling is 85 g/cm^2. We made test runs at fixed proton energy between 10^{16} and 10^{19} eV where the main model features were consecutively switched on to study their effects on the elongation rate. The energy dependence (ln s) of the inelastic cross section decreased the elongation rate to 72±3 g/cm^2. The scaling violation in the fragmentation region generated by the KNP model decreased the value further to 57±2 g/cm^2. When the nuclear target effects are accounted for in the KNP model we then get the final value of 52±2 g/cm^2 given in Sec. III B. The effect of scaling violation is smaller in the minijet model, but the increase of inelasticity is amplified by the nuclear target effect, giving the final value of 55 g/cm^2 for that model.

A large fraction of heavy nuclei in the cosmic-ray flux is not unexpected on the basis of shock acceleration models with maximum energy for singly charged particles below the Fly's Eye range. An increase in the number of protons as energy increases through the range covered by Fly's Eye may point to the increasing importance of an extragalactic source. We note in this context that all data on the cosmic-ray spectrum are consistent with a change in slope at an energy above 10 EeV [55–58]. There is also some evidence for a dip in the spectrum at an energy somewhat below this. If this dip and flattening are interpreted as the appearance of an extragalactic cosmic-ray source, then the trend of the composition is certainly consistent with this interpretation. It is, however, unclear whether these effects could be due to energy resolution or other systematics. In any case, the statistical strength of the evidence for a dip and flattening is still weak. Further confirmation requires significant improvement in statistics above 10 EeV and must await results from giant air-shower experiments such as AGASA (Akeno giant air-shower array [59]), the high-resolution Fly's Eye [60], EAS-1000 [61], and others [62].

[1] K. Asakimori et al., in Proceedings of the 22nd International Cosmic Ray Conference, Dublin, Ireland, 1991, edited by M. Cawley et al. (Dublin Institute for Advanced Study, Dublin, 1992), Vol. 2, p. 57.

[2] G.F. Krymsky, Dokl. Akad. Nauk SSR 234, 1306 (1977) [Sov. Phys. Dokl. 22, 327 (1977)].

[3] W.I. Axford, E. Leer, and G. Skadron, in Proceedings of the 15th International Cosmic Ray Conference, Plovdiv, Bulgaria, 1977 (Bulgarian Academy of Sciences, Plovdiv, 1977), Vol. 11, p. 132.

[4] A.R. Bell, Mon. Not. R. Astron. Soc. 182, 147 (1978).

[5] R.D. Blandford and J.P. Ostriker, Astrophysics J. Lett. 221, L29 (1978).

[6] J.R. Jokipii and G. Morfill, in Astrophysical Aspects of the Most Energetic Cosmic Rays, edited by M. Nagano and F. Takahara (World Scientific, Singapore, 1991), p. 261.

[7] W.I. Axford, in Astrophysical Aspects of the Most Energetic Cosmic Rays [6], p. 406.

[8] J.R. Jokipii, Astrophys. J. 313, 842 (1987).

[9] W.H. Ip and W.I. Axford, in Particle Acceleration in Cosmic Plasmas, Proceedings of the Conference, Newark, DE, 1991, edited by G.P. Zank and T.K. Gaisser, AIP Conf. Proc. No. 264 (AIP, New York, 1992).

[10] H.J. Völk and P.L. Biermann, Astrophys. J. Lett. 333, L65 (1988).

[11] R. Silberberg, S.H. Tsao, M.M. Shapiro, and P.L. Biermann, Astrophys. J. 363, 265 (1990).

[12] A.M. Hillas, in Proceedings of the 16th International Cosmic Ray Conference, Kyoto, Japan, 1979, edited by S. Miyake (University of Tokyo, Tokyo, 1979), Vol. 8, p. 7.

[13] R.J. Protheroe and A.P. Szabo, Phys. Rev. Lett. 69, 2885 (1992).

[14] J. Linsley and A.A. Watson, Phys. Rev. Lett. 46, 459 (1981).

[15] R.M. Baltrusaitis et al., Nucl. Instrum. Methods A240, 410 (1985).

[16] G.L. Cassiday, Annu. Rev. Nucl. Part. Sci. 35, 321 (1985).

[17] G.L. Cassiday et al., Astrophys. J. 356, 669 (1990).

[18] J. Linsley, in Proceedings of the 17th International Cosmic Ray Conference, Paris, France, 1981 (CEN, Saclay, 1981), Vol. 11, p. 254.

[19] CDF Collaboration, F. Abe et al., Phys. Rev. D 41, 2330 (1990).

[20] T.K. Gaisser et al., in Proceedings of the 21st International Cosmic Ray Conference, Adelaide, Australia, 1989, edited by R. J. Protheroe (Graphic Services, North Field, South Australia, 1990), Vol. 8, p. 55.

[21] T.K. Gaisser et al., in Proceedings of the 22nd International Cosmic Ray Confernece [1], Vol. 4, p. 413.

[22] S. Tilav, Ph.D. thesis, University of Delaware, 1991.

[23] T.K. Gaisser, in International Workshop on Techniques to Study Cosmic Rays with Energies Greater than 10^{19} eV, edited by J. Cronin, A. A. Watson, and M. Boratav [Nucl. Phys. B (Proc. Suppl.) 28B, 61 (1992)].

[24] Yu.M. Shabelski, R.M. Weiner, G. Wilk, and Z. Wlodarczyk, J. Phys. G. 18, 1281 (1992).

[25] L.D. Landau, Men of Physics: L.D. Landau-II, edited by D. ter Haar (Pergamon, New York, 1969), pp. 131–151.

[26] G. Cocconi, L. Koester, and D.H. Perkins, LRL Report No. UCID-1444, 1960 (unpublished).

[27] J. Wdowczyk and A.W. Wolfendale, Nature (London) 306, 347 (1983).

[28] G.N. Fowler, A. Vourdas, R.M. Weiner, and G. Wilk, Phys. Rev. D 35, 870 (1987).

[29] G. Wilk and Z. Wlodarczyk, in Proceedings of the VII International Symposium on Very High Energy Cosmic Ray Interactions, Ann Arbor (unpublished).

[30] B.Z. Kopeliovich, N.N. Nikolaev, and I.K. Potashnikova, Phys. Rev. D 39, 769 (1989).

[31] L.N. Lipatov, Zh. Eksp. Teor. Fiz. 90, 1536 (1986) [Sov. Phys. JETP 63, 904 (1986)].

[32] M.O. Azaryan, S.R. Gevorkyan, and E.A. Mamidzanyan, Yad. Fiz. 20, 398 (1974) [Sov. J. Nucl. Phys. 20, 213 (1975)].

[33] R.J. Glauber and G. Matthiae, Nucl. Phys. B21, 135 (1970).

[34] T.K. Gaisser and F. Halzen, Phys. Rev. Lett. 54, 1754 (1987).

[35] L. Durand and H. Pi, Phys. Rev. Lett. 58, 303 (1987).

[36] L. Durand and H. Pi, Phys. Rev. D 40, 1436 (1989).

[37] G. Pancheri and Y. Srivastava, in Physics Simulations at High Energy, edited by V. Barger, T. Gottschalk, and F. Halzen (World Scientific, Singapore, 1987), p. 56.

[38] X.-N. Wang and M. Gyulassy, Phys. Rev. D 44, 3501 (1991).

[39] T.K. Gaisser and T. Stanev, Phys. Lett. B 219, 375 (1989).

[40] V.V. Anisovich, M.N. Kobrinsky, J. Nyiri, and Yu. A. Shabelski, Quark Model and High Energy Collisions (World Scientific, Singapore, 1985).

[41] G. Wilk, Soltan Institute for Nuclear Studies Report No. SINS 2075/P-VIII/A, 1988 (unpublished).

[42] A. Capella and J. Tran Thanh Van, Z. Phys. C 10, 249 (1981).

[43] R.W. Ellsworth, T.K. Gaisser, T. Stanev, and G.B. Yodh, Phys. Rev. D 26, 336 (1982).

[44] A.M. Hillas, in Proceedings of the 17th International Cosmic Ray Conference [18], Vol. 8, p. 193.

[45] J. Engel, T.K. Gaisser, P. Lipari, and T. Stanev, Phys. Rev. D 46, 5013 (1992).

[46] K. Greisen, Prog. Cosmic Ray Phys. 3, 1 (1956).

[47] T.K. Gaisser, in Proceedings of the 21st International Cosmic Ray Conference [20], Vol. 10, p. 312.

[48] R. Walker and A.A. Watson, J. Phys. G 7, 1297 (1981).

[49] T. Kifune, in Proceedings of the 21st International Cosmic Ray Conference [20], Vol. 11, p. 75.

[50] R.M. Baltrusaitis et al., Phys. Rev. Lett. 52, 1380 (1984).

[51] E. Leader and U. Maor, Phys. Lett. 43B, 505 (1973).

[52] M.M. Block, F. Halzen, and B. Margolis, Phys. Rev. D 45, 839 (1992).

[53] T.K. Gaisser, U.P Sukhatme, and G.B. Yodh, Phys. Rev. D **36**, 1350 (1987).

[54] T. Chou and C.N. Yang, in *Proceedings of the 2nd International Conference on High Energy Physics and Nuclear Structure*, Rehovot, Israel, edited by G. Alexander (North-Holland, Amsterdam, 1967).

[55] M.A. Lawrence, R.J.O. Reid, and A.A. Watson, J. Phys. G **17**, 733 (1991).

[56] M. Nagano *et al.*, J. Phys. G **18**, 423 (1992).

[57] N.N. Efimov *et al.*, in *Astrophysical Aspects of the Most Energetic Cosmic Rays*, edited by M. Nagano and F. Takahara (World Scientific, Singapore, 1991), p. 345.

[58] P. Sokolsky, in *Proceedings of the Texas/ESO-CERN Symposium on Relativistic Astrophysics, Cosmology, and Fundamental Physics*, Brighton, England, 1991, edited by J.D. Barrow, L. Mestel, and P.A. Thomas [Ann. N.Y. Acad. Sci. **647** (1991)].

[59] N. Chiba *et al.*, Nucl. Instrum. Methods **A311**, 338 (1992).

[60] E.C. Loh *et al.*, in *Astrophysical Aspects of the Most Energetic Cosmic Rays* [57], p. 345.

[61] G.B. Khristiansen, in *Astrophysical Aspects of the Most Energetic Cosmic Rays* [57], p. 354.

[62] J. Cronin, A.A. Watson, and M. Boratav, in *International Workshop on Techniques to Study Cosmic Rays with Energies Greater than 10^{19} eV* [23].